A Case Study of Investigating Secondary Organic Aerosol Formation Pathways in Beijing using an Observation-based SOA Box Model

Wenyi Yang[1,2], Jie Li[1,2*], Ming Wang[3], Yele Sun[1], Zifa Wang[1,2]

[1] *LAPC, Institute of Atmospheric Physics, Chinese Academy of Sciences, Beijing 100029, China*
[2] *Center for Excellence in Urban Atmospheric Environment, Institute of Urban Environment, Chinese Academy of Sciences, Xiamen 361021, China*
[3] *Nanjing University of Information Science and Technology, Nanjing 210044, China*

ABSTRACT

Current modeling studies have underestimated secondary organic aerosol (SOA) levels in China to a larger degree than over Europe and the United States. In this study, we investigated the SOA formation pathways in urban Beijing for the period of November 7–8, 2014, using an observation-constrained box model in which the multigenerational oxidation processes of volatile organic compounds (VOCs) and intermediate VOCs (IVOCs) and the chemical aging of semi-volatile primary organic aerosols (POAs) were taken into account. The results demonstrated that the SOA formation rate was 30.3 µg m^{-3} day^{-1} in Beijing during the 2-day study period. The contributions of VOCs, IVOCs, and POAs to the SOA levels were 14%, 82%, and 4%, respectively. IVOC contributions were on a scale similar to the magnitude of underestimation in a previous study. The uncertainty analysis showed that SOA levels during the study period were 55.4–102.4 µg m^{-3} (the 25th and 75th percentiles of the sensitivity simulations). The contribution of IVOCs to the SOA formation was dominant compared with that of VOCs and POAs. A more precise IVOC oxidation mechanism can thus improve the performance of the SOA model in China.

Keywords: Secondary organic aerosol; Observation-based SOA model; Formation pathway; Intermediate volatile organic compound; Beijing.

INTRODUCTION

SOA has a significant effect on visibility, atmospheric radiative balance and human health (Liu *et al.*, 2014). Secondary organic aerosols (SOA) have been reported to account for 31%–71% of the OA levels in Beijing (Guo *et al.*, 2014a; Huang *et al.*, 2014; Xu *et al.*, 2015; Sun *et al.*, 2016). Recent studies reported that the SOA concentration in Beijing was more than 17 µg m^{-3}, which was 3–8 times higher than the SOA concentration in other countries (Zhang *et al.*, 2007). The large discrepancies between SOA simulations and observations are attributable to the limited understanding of the complicated chemical and physical processes underlying SOA formation (Hallquist *et al.*, 2009). Traditional two-product mechanisms underestimate the annual SOA concentrations in China by as much as 75% (Jiang *et al.*, 2012). Recently, a volatility basis set (VBS) model was developed using the latest chamber data (Donahue *et al.*, 2006), and this model was expected to

narrow the gap between simulations and measurements. Lin *et al.* (2015) demonstrated that the VBS model only accounted for 30%–36% of the observed OA levels in Beijing; nevertheless, it was a significant improvement over the two-product approach. The performance of the VBS model was different in Switzerland, where the simulated SOA concentration was 73% of the measured concentration (Bergstrom *et al.*, 2012).

Uncertainties in the emissions of SOA precursors are considered a key cause of the underestimations of SOA concentration in China. Miller *et al.* (2016) compared satellite observations and simulations and reported that aromatics were likely underestimated by a factor of 2 over the Pearl River Delta. Furthermore, bottom-up emission inventories indicated that the uncertainties of VOCs and organic carbon emissions in China were ±(68–78)% and ±(258–271)%, respectively (Kurokawa *et al.*, 2013; Li *et al.*, 2017). Therefore, uncertainties in the emission inventory hinder the investigation of SOA formation pathways in China using three-dimensional air quality models.

In this study, we developed a VBS approach-based box model constrained by measured data in Beijing to minimize the effects of emission inventory-induced uncertainties. The newly reported SOA formation mechanisms, including

---

primary organic aerosol aging and IVOC oxidation, were incorporated in the VBS scheme. The contributions from different precursors and formation pathways were quantified, which have not been evaluated in previous SOA simulations in China. Finally, a series of sensitivity simulations were conducted to assess the effects of uncertainties on the estimated SOA levels in Beijing.

DATA AND STUDY METHOD

Measurement Techniques

The observation site is located at the Institute of Atmospheric Physics, Chinese Academy of Sciences (116.4°E, 39.9°N), which is near major roads and is representative of the urban area in Beijing. Submicron aerosol particles were measured on-line on the roof of a two-story building (at an approximate height of 8 m off the ground level) by using an Aerosol Chemical Speciation Monitor (Ng *et al.*, 2011), and CO, NO, O_3, and SO_2 were collected using gas analyzers (Thermo Scientific). The hourly concentrations of gaseous HNO_3 and HONO were measured using the Gas and Aerosol Collector–Ion Chromatography system designed by Dong *et al.* (2012). A newly developed gas chromatography–mass spectrometry–flame ionization detection system was used for on-line measurements of VOCs, including alkenes, alkanes, cycloalkanes, and aromatic hydrocarbons (Wang *et al.*, 2014).

In addition, temperature, pressure, relative humidity, and wind were measured at a meteorological tower at the study site, and the Planetary Boundary Layer (PBL) height was observed using a dual-wavelength (1064 and 532 nm) depolarization lidar (Sugimoto *et al.*, 2000, 2001) developed by the National Institute for Environmental Studies, Japan.

Model Description

Supplemental Fig. S1 presents the conceptual diagram of the SOA scheme components in this study. VOCs (aromatics, terpenes and isoprene), IVOCs and POAs are SOA precursors. Their oxidation reactions with OH, O_3 and NO_3 produced four mixed sets of semi-volatile organic compounds (SVOCs), which were grouped on the basis of

their effective saturation concentrations as follows: 1, 10, 100 and 1000 μg m^{-3} at 298 K. SVOCs generated from anthropogenic precursors is allowed to react with OH in the gas phase at a rate constant of 2×10^{-11} cm^3 molecule^{-1} s^{-1} (Donahue *et al.*, 2013), with each reaction resulting in a shift of the compound to the next lower volatility bin.

POAs traditionally treated as non-volatile in the model (Lane *et al.*, 2008; Jiang *et al.*, 2012; Lin *et al.*, 2015). In this study, the POAs referred to here as primary SVOCs (P-SVOCs), which is regarded as semi-volatile and the vapor-phase portion can undergo photochemical oxidation (Robinson *et al.*, 2007). The volatility distribution factors of POAs emission are shown in Base_vol (Table 1), which are taken from experimental results (May *et al.*, 2013a, b, c). The vapor phase P-SVOCs reacts with OH radicals at a rate constant of 4×10^{-11} cm^3 molecule^{-1} s^{-1} and the oxidation products are represented as a mixture of P-SVOCs and SVOCs in the next lower volatility bins (Table S1).

IVOCs refer to organic compounds which have saturation concentration between 10^3 and 10^6 μg m^{-3}, and are usually missing in most of the emission inventories. Recent studies indicate that POAs emissions are accompanied by the emissions of IVOCs, and the additional IVOCs emission is assumed to be 1.5 times of the POAs emission (Robinson *et al.*, 2007). In this study, IVOCs emission was put into the bin of 10^4 μg m^{-3} saturation concentrations, and the rate constant of IVOCs with OH radicals is 4×10^{-11} cm^3 molecule^{-1} s^{-1}. SOA mass yields for the VOCs and IVOCs precursors and volatility bins used in this box model listed in Table S2.

The equilibrium gas–particle partitioning of an organic *i* with effective gas-phase saturation mass concentration C_i^* (μg m^{-3}) over an SOA solution is:

$$\xi_i = \left(1 + \frac{C_i^*}{C_{OA}}\right)^{-1}; \quad C_{OA} = \sum_i C_i \xi_i \quad (1)$$

where the partitioning coefficient ξ_i is the mass ratio of particle-phase *i* to its total mass concentration (in both gas and particle phases), and C_{OA} is the total mass concentration of the absorbing organic material (Donahue *et al.*, 2006).

Table 1. Volatility distribution factors of POAs emissions.

Scenario	POAs species	Emission fraction for volatility bin with C* of				
		0	1	10	100	1000
Base_vol	Gas vehicle	0.27	0.15	0.26	0.15	0.17
	Biomass burning	0.2	0.1	0.1	0.2	0.4
	Others	0.167	0.167	0.243	0.197	0.226
High_vol	Gas vehicle	0.16	0.11	0.21	0.19	0.33
	Biomass burning	0.15	0.05	0.05	0.2	0.55
	Others	0.11	0.093	0.217	0.217	0.363
Low_vol	Gas vehicle	0.34	0.21	0.3	0.1	0.05
	Biomass burning	0.25	0.15	0.15	0.2	0.25
	Others	0.234	0.217	0.27	0.157	0.122

[a] C* is the saturation concentration of each volatility bin.
[b] C* = 0 means nonvolatile.
[c] Others mean other anthropogenic emission sources.
[d] the distribution factors of POAs emissions are taken from May *et al.* (2003a, b, c).

For POAs and IVOCs emissions, we used the enthalpy of vaporization (ΔH_{vap}) values from May *et al.* (2013) for biomass burning and Ranjan *et al.* (2012) for anthropogenic emissions. This method has been used in previous studies (Murphy and Pandis, 2009). POAs includes 5-volatility bins ranging from 10^{-1} to 10^3 µg m^{-3} saturation mass concentration (C_i^*), which roughly covers the volatility range of semi-volatile organic compounds (SVOCs). IVOCs are put into the sixth bin with 10000 µg m^{-3} C_i^*.

In this study, the method constraining box model by observations is taken from previous studies like Kanaya *et al.* (2009) and Li *et al.* (2011 and 2015). The observed O$_3$, CO, SO$_2$, NO, NO$_2$, HONO, HNO$_3$, VOCs, temperature, Boundary layer (BL) height were averaged or interpolated with a time resolution of 5 min as constraints of the model. We assumed that the values of these observed parameters in this 5-time step were constant and input the box model. The 5-min averaged photolysis rated (J-value) was calculated by an accurate radiative transfer model (TUV4.5), which has been validated on atmospheric oxidation capacity in Beijing (Li *et al.*, 2011). In details, the BL height was derived from the NIES two-wavelength aerosol Mie-lidar (532 and 1064 nm). The 5-min NO$_2$ observations were measured by an Aerodyne CAPS NO$_2$ monitor (Ge *et al.*, 2013). This instrument determines NO$_2$ by directly measuring optical absorption of NO$_2$ at 450 nm in the blue region of electromagnetic spectrum and avoids overestimation of NO$_2$ measured by the photolysis-chemiluminescence monitors (Alpert *et al.*, 1997). The hourly NO observation was from a commercial instrument (Model 42CTL, Thermo Electron

Co.). As precursors of OH, concentrations of gaseous HNO$_3$ and HONO were measured using a Gas and Aerosol Collector with an Ion-exchange Chromatography (GAC-IC) system designed by Dong *et al.* (2012). CBMZ on gas-chemistry employed 133 reactions for 53 species and has been described by Zaveri *et al.* (1999). VOCs from GC-MS/FID (Wang *et al.*, 2014) was mapped into CBMZ lumped mechanism according to suggestions by Yarwood *et al.* (2005) in the CAMx (http://www.camx.com/) user manual as shown in Table 2. POAs and SOA fractions were determined based on positive matrix factorization analysis of Aerosol Chemical Speciation Monitor data and are taken from Sun *et al.* (2016a, b). The hydrocarbon-like OA from heavy-duty vehicle emission, cooking OA, and biomass burning were considered as POAs which were used to constrain the box model. The emission rates of VOCs, NO$_x$, and POAs were obtained from Zhang *et al.* (2009).

In physical processes, we only included the emissions and dry/wet deposition by assuming to be uniformly mixed in the mixing layer. This scheme and assumption have been widely used in the observation-based box-model (Zhang and Carmichael, 1999; Kanaya *et al.*, 2009; Li *et al.*, 2011, 2015). The lidar observations showed that pollutants have been mixed in the mixing layer. The observed wind velocity was only 1–2 m s^{-1} in the study period, which suggested that horizontal transport likely had no significant impact on concentrations in 5-min time step.

The initial time was set to 00:00 local standard time (LST), and each 1-day calculation was repeated three times to spin up the diurnal variations in the concentration of

Table 2. Assignment from VOC Species to CBMZ Model Species.

Model species		Measured compounds
Name	Description	
ETHA	ethane	ethane*1
ETHE	ethene	ethane*1
PAR	paraffin carbon bond (C-C)	propane*3 + i-butane*4 + n-butane*4 + i-pentane*5 + n-pentane*5 + 2-methylpentane*6 + n-hexane*6 + 2,2-dimethylbutane*6 + 2,3-dimethylbutane*6 + cyclopentane*5 + 3-methylpentane*6 + propene*1 + 2,4-dimethylpentane*7 + methylcyclopentane*6 + 2-methylhexane*7 + 2,3-dimethylpentane*7 + cyclohexane*6 + 3-methylhexane* 7 + n-heptane*7 + methylcyclohexane*7 + 2,3,4-trimethylpentane*8 + 2-methylheptane*8 + 3-methylheptane**8 + trans-2-butene*2 + n-octane*8 + n-nonane*9 + n-decane*10 + 1-butene*2 + trans-2-pentene*3 + cis-2-butene*2 + 1-pentene*3 + cis-2-pentene*3 + 1-hexene*4 + ethylbenzene*1 + i-propylbenzene*2 + n-propylbenzene*2 + 1,3,5-trimethylbenzene*1 + 1,2,4-trimethylbenzene*1 + m-ethyltoluene*1 + 1,2,4-trimethylbenzene*1 + p-ethyltoluene*1 + o-ethyltoluene*1
OLET	terminal olefin carbon bond (R-C = C)	propene*1 + 1-butene*1 + 1,3-butadiene*2 + 1-pentene*1 + 1-hexene*1 + styrene*0.5
OLEI	internal olefin carbon bond (R-C = C-R)	trans-2-butene*1 + cis-2-butene*1 + trans-2-pentene*1 + cis-2-pentene*1
TOL	toluene and other monoalkyl aromatics	benzene*1 + toluene*1 + ethylbenzene*1 + styrene*1 + i-propylbenzene*1 + i-propylbenzene*1
XYL	xylene and other polyalkyl aromatics	m/p-xylene*1 + o-xylene*1 + m-ethyltoluene*1 + 1,3,5-trimethylbenzene*1 + p-ethyltoluene*1 + 1,2,4-trimethylbenzene*1 + o-ethyltoluene*1 + 1,2,3-trimethylbenzene*1
ISOP	isoprene	isoprene*1

unmeasured species. The results for November 7 and 8, 2014, are presented in the subsequent section.

RESULTS AND DISCUSSION

Observations of VOCs

Fig. 1 presents the observed hourly benzene, toluene, xylene, and isoprene concentrations in Beijing. In general, these VOC species varied diurnally, with a daytime minimum and a midnight maximum. The peak values of benzene, toluene, xylene, and isoprene were 2.5, 6.3, 3.4, and 0.24 ppb, respectively, at 04:00 on November 8, 2014. The decreased concentration at 12:00 was caused by a deeper afternoon boundary layer and enhanced photochemical reactions, which converted more VOCs into semi-VOCs. Compared to other observations, the concentration of single ring aromatics in Beijing is more than twice that measured in Los Angeles and Paris (Borbon *et al.*, 2013), and the

concentration of isoprene in Beijing was usually below 0.2 ppb, which is only less than one tenth of that in southeastern United States (Xiong *et al.*, 2015). This difference indicates that anthropogenic VOCs may be a more important role in SOA formation in Beijing than in other cities. Fig. 2 presents the observed concentrations of POAs, SOA, NO_x and BL height at Beijing in the study period. Observed POAs in Beijing reached the maximum at 00:00–02:00 and the minimum around 12:00. This POAs diurnal variation presents an anticorrelation with BL height. At 23:00 on November 8, BL height was only 400 m and POAs concentrations even exceeded $50 \, \mu g \, m^{-3}$ at this moment.

Comparison between Simulations and Observations

OH radicals are key oxidants that determine the transformation rate from gaseous precursors to SOA. Unfortunately, OH was rarely observed in Beijing because
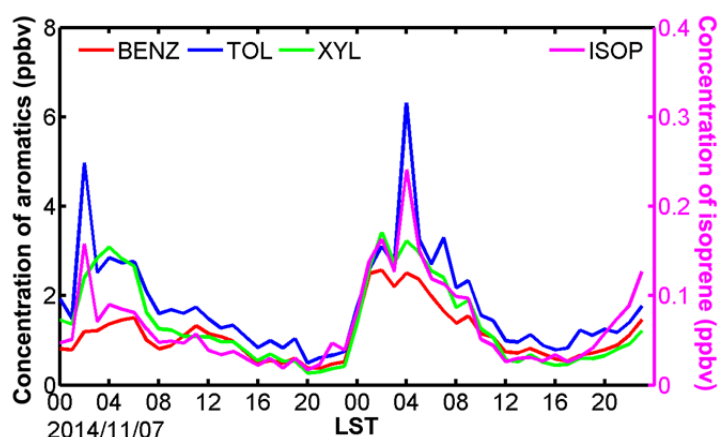

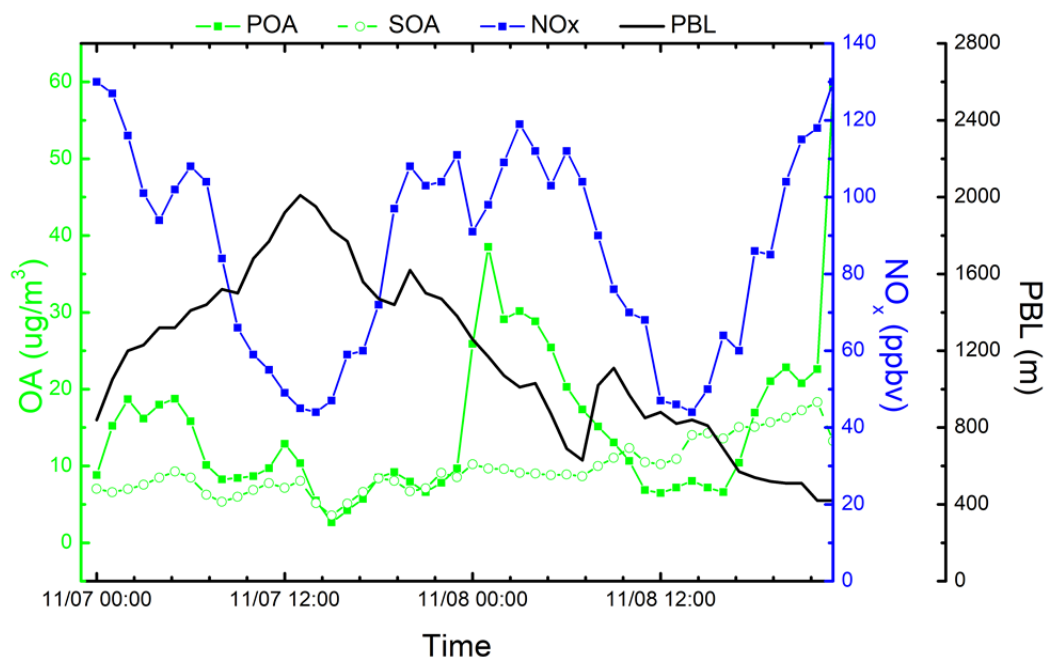**Fig. 1.** Observed single-ring aromatics (benzene, toluene, and xylene) and isoprene mixing ratios (ppbv).

Fig. 2. Observed hourly OA ($\mu g \, m^{-3}$) and NO_x (ppbv) concentrations and BL height (m) in this study.

it was very hard. In this study, we employed the calculated OH value constrained by its mostly precursors' observations (NO$_x$, VOCs, HCHO, HONO, O$_3$). Similar calculation was presented by Kanaya *et al.* (2009) in Mt. Tai, and Liu *et al* (2012) in Beijing, who found that this didn't bring significant errors. Although there were few OH observations in Beijing, we collected OH "observations" in August 2007 (Liu *et al.*, 2012) and October 13–17, 2000 (Ren *et al.*, 2004), in Beijing. Fig. 3 showed the comparison between observed OH in August, October and calculated OH in November in this study. We found that simulated OH was a little less than observation in October, because the driving energy of OH production (UV-B radiation) decreased from October to November rather than the model itself. The same reasons resulted in the 80% decrease of observed OH from August to October. In conclusion, the simulated OH reasonably reproduced the OH in the study period.

IVOC concentrations are rarely measured worldwide. Nevertheless, we compared the ratio of simulated IVOCs to single-ring aromatics in Beijing with a few observations in other countries. In this study, the mean simulated IVOC mass concentration was 48.3 µg m^{-3}, which was nearly two times that of the measured concentration of single-ring aromatics. The IVOC/single-ring aromatics ratio is comparable and slightly higher than that observed in California (1.0–1.2) during 2010 (Zhao *et al.*, 2014).

SOA Formation Rates in Beijing

Fig. 4(a) shows the mean contribution to the net SOA production from three formation pathways in base simulation during daytime. In this 2-day simulation, the total daytime (08:00–17:00 LST) SOA net production was 60.6 µg m^{-3}. SOA production by the oxidation of IVOCs (SOA^{IV}) was the dominant pathway, which accounted for 82% (49.7 µg m^{-3})

Fig. 4. (a) The averaged contribution from each pathway during daytime (08:00–17:00) and (b) the hourly net SOA production rate from different pathways. Note that SOA^V, SOA^{IV} and SOA^P represents the SOA from oxidation of VOCs, IVOCs and semi-volatile POA.

of the total SOA concentration. The magnitude of this contribution is similar to that of the underestimations reported in a previous study (Lin *et al.*, 2015). The traditional SOA formation pathway from the oxidation of aromatics (SOA^V) only contributed 14% (8.5 µg m^{-3}), and the aging of the gas-phase POAs (SOA^P) only accounted for 4% (2.4 µg m^{-3}). The hourly net SOA production had a single-peak distribution pattern as shown in Fig. 4(b). After 08:00, the hourly SOA formation increased rapidly to a maximum of 5.5 µg m^{-3} at 11:00, which subsequently decreased to a minimum of 0.5 µg m^{-3} at night (not shown in Fig. 4(b)). The hourly SOA^V, SOA^{IV}, and SOA^P levels ranged from 0.1 to 0.9, 0.3 to 5.3, and < 0.1 to 0.3 µg m^{-3}, respectively. The average SOA levels during the early afternoon (12:00–15:00 LST) were > 3.3 µg m^{-3} h^{-1}, which is four times of those reported in California (Zhao *et al.*, 2014) because of the abundant SOA precursors present in Beijing.

Uncertainties in the Estimated SOA Formation Rates from Different Pathways

As shown in Table 3, 39 sensitivity simulations were conducted to evaluate the uncertainties of estimated SOA formation rates. As mentioned previously, the uncertainty in the POAs emission rate was ± 271% (Kurokawa *et al.*, 2013). Two sensitivity simulations (Table 3, S01 and S02)
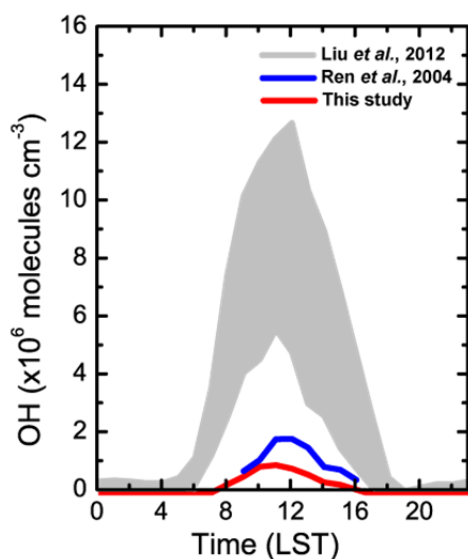
Fig. 3. Simulated diurnal OH concentrations in Nov. in Beijing. Also shown are observed OH in Aug. and Oct. in Beijing. The grey area shows the 20-day average diurnal variation of the OH radical with the hourly standard deviations.
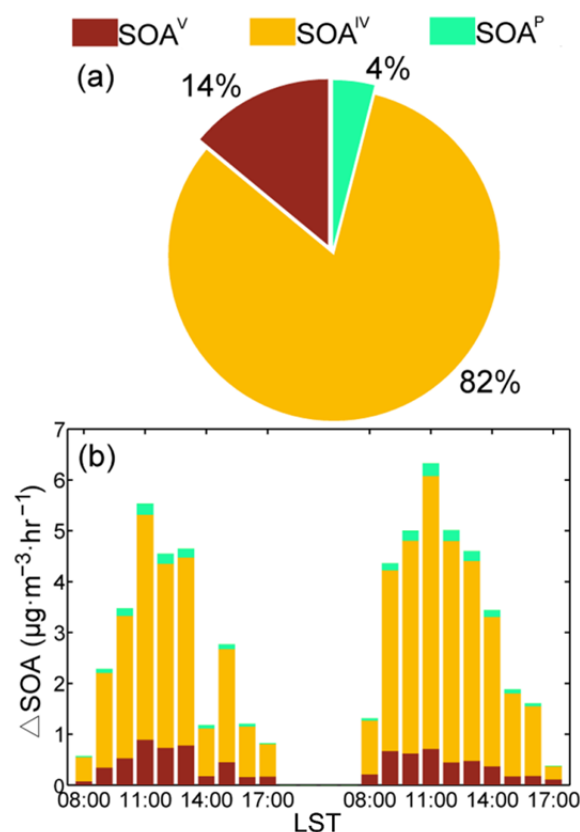
Table 3. Sensitive simulation descriptions.

Scenarios	Description
Base	Base_vol scenario, IVOCs/POAs = 1.5 for all emission sectors
S01	Same as Base, but POAs emission is twice that of Base
S02	Same as Base, but POAs emission is half that of Base
S03	Same as Base, but POAs volatility distribution use High_vol scenario
S04	Same as Base, but POAs volatility distribution use Low_vol scenario
S05	Same as Base, but IVOCs/POAs = 4.5 for transport emission, and IVOCs/POAs = 1.5 for other anthropogenic emissions
S06	Same as Base, but no IVOCs emission
S07	POAs is regarded as non-volatile compounds, and no IVOCs emission
S08	POAs emission is twice that of Base, High_vol scenario
S09	POAs emission is half that of Base, High_vol scenario
S10	POAs emission is twice that of Base, Low_vol scenario
S11	POAs emission is half that of Base, Low_vol scenario
S12	IVOCs/POAs = 2.0 for transport emission
S13	IVOCs/POAs = 2.5 for transport emission
S14	IVOCs/POAs = 3.0 for transport emission
S15	IVOCs/POAs = 3.5 for transport emission
S16	IVOCs/POAs = 4.0 for transport emission
S17	High_vol scenario, and IVOCs/POAs = 2.0 for transport emission
S18	High_vol scenario, and IVOCs/POAs = 2.5 for transport emission
S19	High_vol scenario, and IVOCs/POAs = 3.0 for transport emission
S20	High_vol scenario, and IVOCs/POAs = 3.5 for transport emission
S21	High_vol scenario, and IVOCs/POAs = 4.0 for transport emission
S22	Low_vol scenario, and IVOCs/POAs = 2.0 for transport emission
S23	Low_vol scenario, and IVOCs/POAs = 2.5 for transport emission
S24	Low_vol scenario, and IVOCs/POAs = 3.0 for transport emission
S25	Low_vol scenario, and IVOCs/POAs = 3.5 for transport emission
S26	Low_vol scenario, and IVOCs/POAs = 4.0 for transport emission
S27	POAs emission is 2.5 times that of Base
S28	POAs emission is 1.5 times that of Base
S29	POAs emission is 2.5 times that of Base, High_vol scenario
S30	POAs emission is 1.5 times that of Base, High_vol scenario
S31	POAs emission is 2.5 times that of Base, Low_vol scenario
S32	POAs emission is 1.5 times that of Base, Low_vol scenario
S33	SOAs mass yields under high-NO_x conditions multiply by 1.2
S34	anthropogenic SOA aging reaction rate use 1×10^{-11} cm^3 molecule^{-1} s^{-1}
S35	anthropogenic SOA aging reaction rate use 4×10^{-11} cm^3 molecule^{-1} s^{-1}
S36	anthropogenic SOA aging reaction rate use 4×10^{-12} cm^3 molecule^{-1} s^{-1}
S37	the concentration of OH radical multiplied by 2
S38	the concentration of OH radical multiplied by 3
S39	the concentration of OH radical multiplied by 5

were conducted to evaluate the effects of POAs emission rate uncertainty. The POAs emission rates in S01 and S02 were 200% and 50% those in the base case, respectively. The total SOA production in S01 and S02 was 69.8 and 55.0 µg m^{-3}, respectively (Figs. 5(a) and 5(b)). The SOA^{IV} formation in S01 and S02 were 6.3 µg m^{-3} more than that in the base case (49.7 µg m^{-3}) and 2.8 µg m^{-3} less than that in the base case, respectively. The change in the POAs emission rates not only affected the contributions from SOA^P but also affected the total SOA formation through gas-particle partitioning.

POAs volatility distribution factors, as listed in the Base_vol scenario (Table 1), were used in a three-dimensional chemical transport model (Koo *et al.*, 2014). May *et al.*

(2013a, b, c) reported a wide range of values of POAs volatility distribution factors. In this study, two sensitivity simulations, in which the POAs have the highest (S03, High_vol scenario in Table 1) and the lowest (S04, Low_vol scenario in Table 1) volatilities, were conducted to evaluate the effects of POAs volatility on SOA formation (Table 3). The difference in the portion of gaseous POAs only slightly changed the SOA^P levels (~1 µg m^{-3}) in the base case, S03, and S04 (Figs. 5(c) and 5(d)). Uncertainties in the POAs volatility distribution (May *et al.*, 2013a, b, c) exerted a higher effect on particle-phase POAs than SOA, and the total losses of particle-phase POAs mass in the base case, S03, and S04 were 38.4, 62.3, and 19.2 µg m^{-3}, respectively. The volatility distribution factors can strongly

affect the total OA (including particle-phase SOA and POAs) mass as well as the SOA/OA ratio. In particular, the simulated SOA/OA ratio was largely underestimated in China relative to the measured SOA/OA ratio. Jiang *et al.* (2012) found that the simulated SOA/OA ratio in Beijing in summertime was underestimated to a certain degree of 40% compared with the observations. During the 2-day study period, the SOA/OA ratio in base case, S03, S04 and observation was 38.2%, 39.6%, 36.9% and 42.8%, respectively.

The IVOC emission rate has not been reported in previous bottom-up emission inventories. Robinson *et al.* (2007) suggested a IVOC/POAs emission ratio of almost 1.5 and applied it to three-dimensional modeling studies in Europe and America (Tsimpidi *et al.*, 2010). However, a recent study showed that IVOC emissions could be as much as 4.5 times higher than POAs emissions (Woody *et al.*, 2015). In this study, the higher IVOC emission simulation (Table 3, S05) and no IVOC emission simulation (Table 3, S06) were performed to estimate the extreme influence of IVOCs (Table 3). The total SOA formed in S05 was 139.9 µg m^{-3} (Fig. 5), which was more than two times that in the base case. Without contributions from SOA^{IV} (S06), the total SOA production was only 8.2 µg m^{-3}. The comparison among base case (IVOCs/POA ratio of 1.5), S05 (change the IVOCs/POAs ratio to 4.5 only for transportation sources) and S06 (no IVOCs emission) shown large discrepancy of total SOA production in Beijing. Considering the impacts of IVOCs emission uncertainties on SOA formation, additional studies on IVOCs emissions are warranted to provide additional insights into SOA formation in China.

OH concentrations and the OH aging rates of SOA precursors (4×10^{-11}) were the uncertainty sources in this study. Six sensitivity simulations (S34–S39, Table 3) were conducted to examine the effects of these uncertainties. The different anthropogenic SOA aging rate by OH radicals lead to the differences in the total net production of SOA. However, the relative contribution from each pathway nearly the same (Fig. 6).

Fig. 7 presents the boxplots of SOA formation from three pathways based on all sensitivity simulations (including S01–S39). The median value was regarded as the SOA production rate. In this study, the 25th and 75th percentiles represent the varying ranges of SOA formation rates, which account for the uncertainties related to emissions and model parameters. In general, the median SOA formation of S01–S39 during this 2-day study period was 73.8 µg m^{-3}, and the 25th and 75th percentiles was 55.4 µg m^{-3} and 102.4 µg m^{-3}, respectively. The SOA formation from three pathways (SOA^{V}, SOA^{IV}, and SOA^{P}), was 7.7–9.5 µg m^{-3}, 46.7–90.9 µg m^{-3} and 1.0–2.7 µg m^{-3} (25th and 75th percentiles), respectively.

Implications for Three-dimensional SOA Simulations in China

In most current SOA three-dimensional simulations in China, SOA were formed only from VOCs, which were underestimated by approximately 70% compared with the observations in Beijing (Guo *et al.*, 2014b; Lin *et al.*, 2015). In particular, the multigeneration oxidation of VOCs was considered a possible method to improve model performance. Zhang *et al.* (2014) suggested that SOA mass yields under high NO$_x$ conditions may be underestimated by a factor of approximately 1.2 due to vapor losses. In this study, according to the measured VOCs, contributions from the multigeneration oxidation of VOCs were only 14%. Furthermore, corrections in mass yields only increased the predicted SOA^{V} to 9.6 µg m^{-3} and did not alter the relative contribution of VOCs (15%) substantially, indicating that
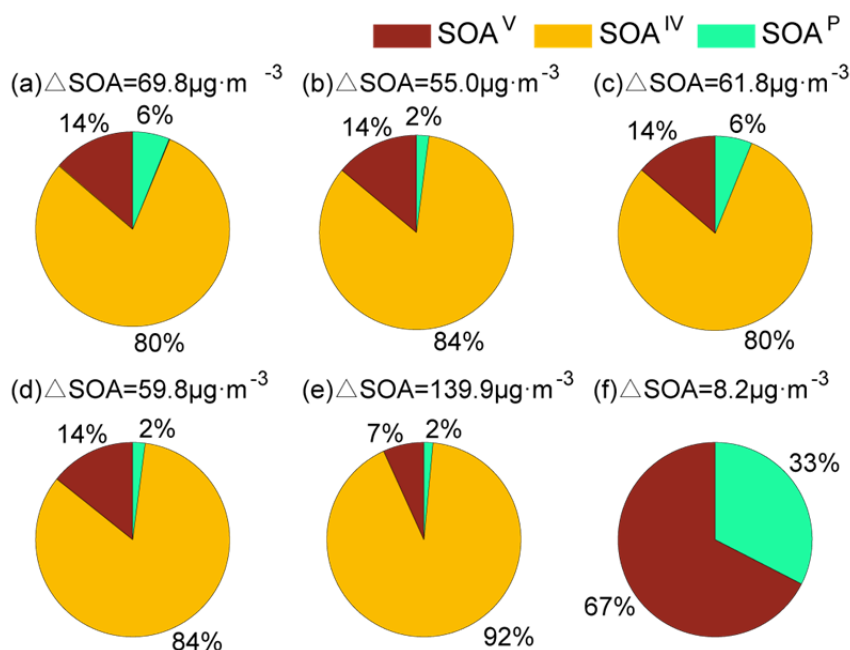

Fig. 5. Net daytime SOA production (µg m^{-3}) from different pathways in the sensitivity simulations ((a)–(f) represents S01–S06 in Table 3, respectively).
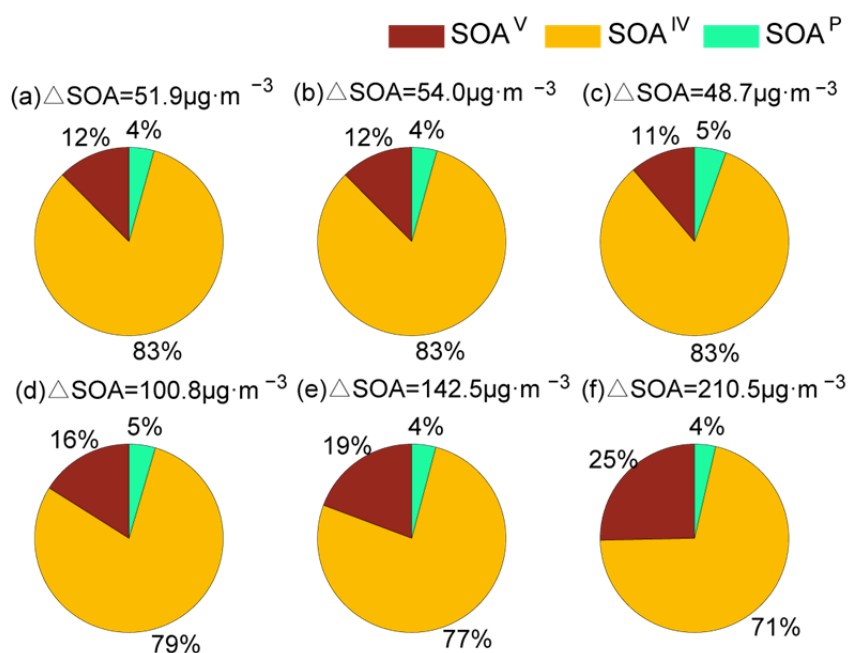
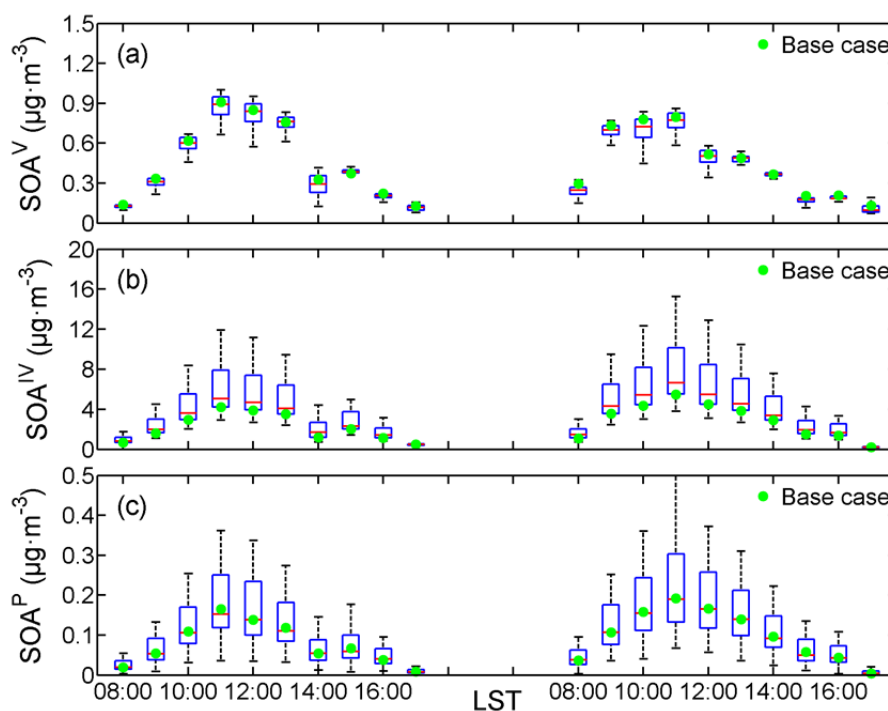**Fig. 6.** The same as Fig. 5, but (a)–(f) refers to S34–S39 in Table 3, respectively.

Fig. 7. Boxplots of the hourly net SOA formation production rates (μg m^{-3} hr^{-1}) from different pathways based on sensitivity simulations including S01–S39 (red line, blue box, whiskers, and markers beyond the range of whiskers represent the median value, 25th and 75th percentiles, the 1.5 interquartile range, and outliers, respectively). The green solid points represent the base case. (a) SOA from oxidation of VOCs, (b) SOA from oxidation of IVOCs and (c) SOA from oxidation of semi-volatile POAs.

the SOA simulations in Beijing may not significantly improve the simulated SOA levels based on the current multigeneration VOC oxidation mechanisms.

The POAs mechanism was expected to largely explain discrepancies between observations and simulations and

could contribute approximately 50% to the total SOA levels in Europe (Bergstrom *et al.*, 2012); however, modeling studies in China have rarely considered this mechanism. In this study, SOA^P accounted for only less than 5% of the total SOA levels in Beijing, which is much less than those

reported in Europe and the United States (Hodzic *et al.*, 2010).

In this study, IVOCs were the most important precursors of SOA. SOA production was remarkably increased through the IVOC mechanism in Beijing, which is expected to reduce the gap between simulations and observations. As mentioned previously, the SOA formed by IVOCs remain a large source of uncertainties (Fig. 7(b)), and the lack of observations in China hinder the selection of correct modeling parameters. The emission sources and reaction rates of IVOCs are required for further identification and quantification.

CONCLUSIONS AND RECOMMENDATIONS

We used an observation-constrained box model and related measurements to examine the current SOA formation in urban Beijing in autumn. In the base case, the total SOA yield during the 2-day study period was 60.6 µg m^{-3}, which is consistent with the yield reported for a previously recommended model configuration. The contributions from the oxidation of VOCs, IVOCs, and semi-volatile POAs (SOA^V, SOA^{IV}, and SOA^P) were 14%, 82%, and 4%, respectively. Considering the uncertainties in the emission rates and POAs volatility distribution factors, the median SOA net production of the sensitivity simulations in this study was 73.8 µg m^{-3} (55.4–102.4 µg m^{-3}). The amount of SOA formed via the three pathways (SOA^V, SOA^{IV}, and SOA^P), the SOA formation was 7.7–9.5 µg m^{-3}, 46.7–90.9 µg m^{-3}, and 1.0–2.7 µg m^{-3}, respectively. IVOC oxidation was the major contributor to SOA production in Beijing during the study period. The present finding, which has not been reported for previous simulations in China, is likely to improve the predictive accuracy of three-dimensional SOA models in the nation.

ACKNOWLEDGMENTS

SUPPLEMENTARY MATERIAL

Supplemental Tables S1 presents the SOA chemical aging. Table S1 presents SOA mass yields for the VOCs and IVOCs precursors and volatility bins used in this box model. Fig. S1 presents the conceptual diagram of the SOA scheme components. Supplementary data associated with this article can be found in the online version at http://www.aaqr.org.

REFERENCES

Alpert, C., Ramdev, N., George, D. and Loscalzo, J. (1997). Detection if S-Nitrosothiols and other nitric oxide derivatives by photolysis-chemiluminescence spectrometry. *Anal. Biochem.* 245: 1–7.

Bergstrom, R., Denier van der Gon, H.A.C., Prevot, A.S.H.,

Yttri, K.E. and Simpson, D. (2012). Modelling of organic aerosols over Europe (2002-2007) using a volatility basis set (VBS) framework: Application of different assumptions regarding the formation of secondary organic aerosol. *Atmos. Chem. Phys.* 12: 8499–8527.

Borbon, A., Gilman, J., Kuster, W.C., Grand, N., Chevaillier, S., Colomb, A., Dolgorouky, C., Gros, V., Lopez, M., Sarda-Esteve, R., Holloway, J., Stutz, J., Petetin, H., McKeen, S., Beekmann, M., Warneke, C., Parrish, D.D. and Gouw, J.A. (2013). Emission ratios of anthropogenic VOC in northern mid-latitude megacities: Observations vs. emission inventories in Los Angeles and Paris. *J. Geophys. Res.* 118: 2041–2057.

Donahue, N.M., Robinson, A.L., Stanier, C.O. and Pandis, S.N. (2006). Coupled partitioning, dilution and chemical aging of semivolatile organics. *Environ. Sci. Technol.* 40: 2635–2643.

Dong, H.B., Zeng, L.M., Hu, M., Wu, Y.S., Zhang, Y.H., Slanina, J., Zheng, M., Wang, Z.F. and Jansen, R. (2012). Technical Note: The application of an improved gas and aerosol collector for ambient air pollutants in China. *Atmos. Chem. Phys.* 12: 10519–10533.

Ge, B., Sun, Y., Liu, Y., Dong, H., Ji, D., Jiang, Q., Li, J. and Wang, Z. (2013). Nitrogen dioxide measurement by cavity attenuated phase shift spectroscopy (CAPS) and implications in ozone production efficiency and nitrate formation in Beijing, China. *J. Geophys. Res.* 118: 9499–9509.

Guo, S., Hu, M., Zamora, M.L., Peng, J.F., Shang, D.J., Zheng, J., Du, Z.F., Wu, Z.J., Shao, M., Zeng, L.M., Molina, M.J. and Zhang, R.Y. (2014a). Elucidating severe urban haze formation in China. *PNAS* 111: 17373–17378.

Guo, X.S., Situ, S.P., Wang, X.M., Ding, X., Wang, X.M., Yan, C.Q., Li, X.Y. and Zheng, M. (2014b). Numerical modeling analysis of Secondary Organic Aerosol (SOA) combined with the ground-based measurements in the Pearl River Delta region, *Environ. Sci.* 35: 1654–1661. (in Chinese)

Hallquist, M., Wenger, J.C. and Baltensperger, U. (2009). The formation, properties and impact of secondary organic aerosol: Current and emerging issues. *Atmos. Chem. Phys.* 9: 5155–5236.

Hodzic, A., Jimenez, J.L., Madronich, S., Canagaratna, M., DeCarlo, P.F., Kleinman, L. and Fast, J. (2010). Modeling organic aerosols in a megacity: Potential contribution of semi-volatile and intermediate volatility primary organic compounds to secondary organic aerosol formation. *Atmos. Chem. Phys.* 10: 5491–5514.

Huang, R.J., Zhang, Y.L., Bozzetti, C., Ho, K.F., Cao, J.J., Han, Y.M., Daellenbach, K.R., Slowik, J.G., Platt, S.M., Canonaco, F., Zotter, P., Wolf, R., Pieber, S.M., Bruns, E.A., Crippa, M., Ciarelli, G., Piazzalunga, A., Schwikowski, M., Abbaszade, G., Schnelle-Kreis, J., Zimmermann, R., An, Z., Szidat, S., Baltensperger, U., Haddad, I.E. and Prevot, A.S.H. (2014). High secondary aerosol contribution to particulate pollution during haze events in China. *Nature* 514: 218–222.

Jiang, F., Liu, Q., Huang, X.X., Wang, T.J., Zhuang, B.L. and Xie, M. (2012). Regional modeling of secondary

organic aerosol over china using WRF/Chem. *J. Aerosol Sci.* 43: 57–73.

Kanaya, Y., Pochanart, P., Liu, Y., Li, J., Tanimoto, H., Kato, S., Suthawaree, J., Inomata, S., Taketani, F., Okuzawa, K., Akimoto, H. and Wang, Z. (2009). Rates and regimes of photochemical ozone production over Central East China in June 2006: A box model analysis using comprehensive measurements of ozone precursors. *Atmos. Chem. Phys.* 9: 7711–7723.

Koo, B., Knipping, E. and Yarwood, G. (2014). 1.5-Dimensional volatility basis set approach for modeling organic aerosol in CAMx and CMAQ. *Atmos. Environ.* 95: 158–164.

Kurokawa, J., Ohara, T., Morikawa, T. and Hanayama, S. (2013). Emissions of air pollutants and greenhouse gases over Asian regions during 2000-2008: Regional Emission inventory in Asia (REAS) version 2. *Atmos. Chem. Phys.* 13: 11019–11058.

Lane, T.E., Donahue, N.M. and Pandis, S.N. (2008). Simulating secondary organic aerosol formation using the volatility basis-set approach in a chemical transport model. *Atmos. Environ.* 42: 7439–7451.

Li, J., Wang, Z. and Xiang, W. (2011). Daytime atmospheric oxidation capacity of urban Beijing under polluted conditions during the 2008 Beijing Olympic Games and the impact of aerosols. *SOLA* 7: 73–76.

Li, J., Dong, H.B., Zeng, L.M., Zhang, Y.H., Shao, M., Wang, Z.F., Sun, Y.L. and Fu, P.Q. (2015). Exploring possible missing sinks of nitrate and its precursors in current air quality models—A case simulation in the Pearl River Delta, China, using an observation-based box model. *SOLA* 11: 124–128.

Li, M., Zhang, Q., Kurokawa, J.I., Woo, J.H., He, K., Lu, Z., Ohara, T., Song, Y., Streets, D.G., Carmichael, G.R., Cheng, Y., Hong, C., Huo, H., Jiang, X., Kang, S., Liu, F., Su, H. and Zheng, B. (2017). MIX: A mosaic Asian anthropogenic emission inventory under the international collaboration framework of the MICS-Asia and HTAP. *Atmos. Chem. Phys.* 17: 935–963.

Lin, J., An, J.L., Qu, Y., Chen, Y., Li, Y., Tang, Y.J., Wang, F. and Xiang, W.L. (2015). Local and distant source contributions to secondary organic aerosol in the Beijing urban area in summer. *Atmos. Environ.* 124: 176–185.

Liu, Y.Z., Jia, R., Dai, T., Xie, Y.K. and Shi, G.Y. (2014). A Review of aerosol optical properties and radiative effects. *J. Meteorolog. Res.* 28: 1003–1028.

Liu, Z., Wang, Y., Gu, D., Zhao, C., Huey, L.G., Stickel, R., Liao, J., Shao, M., Zhu, T., Zeng, L., Amoroso, A., Costabile, F., Chang, C.C. and Liu, S.C. (2012). Summertime photochemistry during CAREBeijing-2007: ROx budgets and O$_3$ formation. *Atmos. Chem. Phys.* 12: 7737–7752.

May, A.A., Levin, E.J.T., Hennigan, Ilona, C.J.R., Taehyoung, L., Collett, J.L., Jimenez, J.L., Kreidenweis, S.M. and Robinson, A.L. (2013). Gas-particle partitioning of primary organic aerosol emissions: 3. Biomass burning. *J. Geophys. Res.* 118: 11327–11338.

May, A.A., Presto, A.A., Hennigan, C.J., Nguyen, N.T., Gordon, T.D. and Robinson, A.L. (2013a). Gas-particle

partitioning of primary organic aerosol emissions: (1) gasoline vehicle exhaust. *Atmos. Chem. Phys.* 77: 128–139.

May, A.A., Presto, A.A., Hennigan, C.J., Nguyen, N.T., Gordon, T. and DRobinson, A. (2013b). Gas-particle partitioning of primary organic aerosol emissions: (2) diesel vehicles. *Environ. Sci. Technol.* 47: 8288–8296.

Miller, C.C., Jacob, D.J., Abad, G.G. and Chance, K. (2016). Hotspot of glyoxal over the Pearl River delta seen from the OMI satellite instrument: Implications for emissions of aromatic hydrocarbons. *Atmos. Chem. Phys.* 16: 4631–4639.

Murphy, B.N. and Pandis, S.N. (2009). Simulating the formation of semivolatile primary and secondary organic aerosol in a regional chemical transport model. *Environ. Sci. Technol.* 43: 4722–4728.

Ng, N.L., Herndon, S.C., Trimborn, A., Canagaratna, M.R., Croteau, P.L., Onasch, T.B., Sueper, D., Worsnop, D.R., Zhang, Q., Sun, Y.L. and Jayne, J.T. (2011). An Aerosol Chemical Speciation Monitor (ACSM) for routine monitoring of the composition and mass concentrations of ambient aerosol. *Aerosol Sci. Technol.* 45: 780–794.

Pathak, R.K., Presto, A.A., Lane, T.E., Stanier, C.O., Donahue, N.M. and Pandis, S.N. (2007). Ozonolysis of α-pinene: Parameterization of secondary organic aerosol mass fraction. *Atmos. Chem. Phys.* 7: 3811–3821.

Ren, X.R., Wang, L.X., Wang, H.X. and Miao, G.F. (2004). Conversion rates of surface HOx radicals in Beijing City. *Chin. Geog. Sci.* 14: 34–38.

Robinson, A.L., Donahue, N.M., Shrivastava, M., Weitkamp, E.A., Sage, A.M., Grieshop, A.P., Lane, T.E., Pierce, J.R. and Pandis, S.N. (2007). Rethinking organic aerosols: Semivolatile emissions and photochemical aging. *Science* 315: 1259–1262.

Shrivastava, M.K., Lane, T.E., Donahue, N.M., Pandis, S.N. and Robinson, A.L. (2008). Effects of gas particle partitioning and aging of primary emissions on urban and regional organic aerosol concentrations. *J. Geophys. Res.* 113: D18301.

Shrivastava, M., Fast, J., Easter, R., Gustafson Jr, W.I., Zaveri, R.A., Jimenez, J.L., Saide, P. and Hodzic, A. (2011). Modeling organic aerosols in a megacity: Comparison of simple and complex representations of the volatility basis set approach. *Atmos. Chem. Phys.* 11: 6639–6662.

Sugimoto, N., Matsui, I., Liu, Z., Shimizu, A., Tamamushi, I. and Asai, K. (2000). Observation of aerosols and clouds using a Two-wavelength polarization lidar during the Nauru99 experiment. *Sea Sky* 76: 93–98.

Sugimoto, N., Matsui, I., Liu, Z., Shimizu, A., Asai, K., Yoneyama, K. and Katsumata, M. (2001). Latitudinal distribution of aerosols and clouds in the western Pacific observed with a lidar on board the research vessel Mirai, *Geophys. Res. Lett.* 28: 4187–4190.

Sun, Y.L., Du, W., Fu, P.Q., Wang, Q.Q., Li, J., Ge, X.L., Zhang, Q., Zhu, C.M., Ren, L.J., Xu, W.Q., Zhao, J. Han, T.T., Worsnop D.R. and Wang, Z.F. (2016a). Primary and secondary aerosols in Beijng in winter: Sources, variations and processes. *Atmos. Chem. Phys.* 16: 8309–8329.

Sun, Y.L., Wang, Z.F., Wild, O., Xu, W.Q., Chen, C., Fu, P.Q., Du, W., Zhou, L.B., Zhang, Q., Han, T.T., Wang, Q.Q., Pan, X.L., Zheng, H.T., Li, J., Guo, X.F., Liu, J.G. and Worsnop, D.R. (2016b). "APEC Blue": Secondary aerosol reductions from emission controls in Beijing, *Sci. Rep.* 6: 20668.

Tsimpidi, A.P., Karydis, V.A., Zavala, M. and Lei, W. (2010). Evaluation of the volatility basis-set approach for the simulation of organic aerosol formation in the Mexico City metropolitan area. *Atmos. Chem. Phys.* 10: 525–546.

Wang, M., Zeng, L.M., Lu, S.H., Shao, M., Liu, X.L., Yu, X.N., Chen, W.T., Yuan, B.H., Zhang, Q., Hu, M. and Zhang, Z.Y. (2014). Development and validation of a cryogen-free automatic gas chromatograph system (GS-MS/FID) for online measurements of volatile organic compounds. *Anal. Methods* 6: 9424–9434.

Woody, M.C., West, J.J., Jathar, S.H., Robinson, A.L. and Arunachalam, S. (2015). Estimates of non-tradional secondary organic aerosols from aircraft SVOC and IVOC emissions using CMAQ. *Atmos. Chem. Phys.* 15: 6929–6942.

Xiong, F., McAvey, K.M., Pratt, K.A., Groff, C.J., Hostetler, M.A., Lipton, M.A., Starn, T.K., Seeley, J.V., Bertman, S.B., Teng, A.P., Crounse, J.D., Nguyen, T.B., Wennberg, P.O., Misztal, P.K., Goldstein, A.H., Cuenther, A.B., Koss, A.R., Olson, K.F., Gouw, J.A. de, Baumann, K., Edgerton, E.S., Feiner, P.A., Zhang, L., Miller, D.O., Brune, W.H. and Shepson, P.B. (2015). Observation of isoprene hydroxynitrates in the southeastern United States and implications for the fate of NO_x. *Atmos. Chem. Phys.* 15: 11257–11272.

Xu, Z., Wen, T., Li, X., Wang, J. and Wang, Y. (2015). Characteristics of carbonaceous aerosols in beijing based on two-year observation. *Atmos. Pollut. Res.* 6: 202–208.

Yarwood, G., Rao, S., Yocke, M. and Whitten, G.Z. (2005). Updates to the carbon bound chemical mechanism: CB05. Appendix A. Final Report to the US EPA; EPA Report RT-0400675.

Zaveri, R.A. and Peters, L.K. (1999). A new lumped structure photochemical mechanism for large-scale applications. *J. Geophys. Res.* 104: 30387–30415.

Zhang, Q., Jimenez, J.L., Canagaratna, M.R., Allan, J.D., Coe, H., Ulbrich, I., Alfarra, M.R., Takami, A., Middlebrook, A.M., Sun, Y.L., Dzepina, K., Dunlea, E., Docherty, K., DeCarlo, P.F., Salcedo, D., Onasch, T., Jayne, J.T., Miyoshi, T., Shimono, A., Hatakeyama, S., Takegawa, N., Kondo, Y., Schneider, J., Drewnick, F., Borrmann, S., Weimer, S., Demerjian, K., Williams, P., Bower, K., Bahreini, R., Cottrell, L., Griffin, R.J., Rautiainen, J., Sun, J.Y., Zhang, Y.M. and Worsnop, D.R. (2007). Ubiquity and dominance of oxygenated species in organic aerosols in anthropogenically-influenced Northern Hemisphere midlatitudes. *Geophys. Res. Lett.* 34: L13801.

Zhang, Y. and Carmichael, G.R. (1999). The role of mineral aerosol in tropospheric chemistry in East Asia - A model study. *J. Appl. Meteorol.* 38: 353–366.

Zhao, Y.L., Hennigan, C.J., May, A.A., Tkacik, D.S., Gouw, J.A. de, Gilman, J.B., Kuster, W.C., Borbon, A. and Robinson, A.L. (2014). Intermediate-volatility organic compounds: A large source of secondary organic aerosol. *Environ. Sci. Technol.* 48: 13743–13750.